

Safe Operation of Welded Structure with Cracks at Elevated Temperature

Meri Burzić^{1,*} - Radica Prokić-Cvetković² - Biljana Grujić³ - Ivana Atanasovska⁴ - Živoslav Adamović⁵

¹ Institute "GOŠA", Belgrade, Serbia

² Faculty of Mechanical Engineering, Belgrade, Serbia

³ Innovation Centre, Belgrade, Serbia

⁴ Institute "Kirilo Savić", Belgrade, Serbia

⁵ Faculty of Technical Engineering, Zrenjanin, Serbia

The fatigue crack growth rate parameters and conditions for abrupt fracture of thick joint in steel at room and operating temperature were analysed. Fatigue cracks generated from sharp weld defects are initial cracks that grow through either the weld joint region or the base metal in accordance with Paris law. Service life of a welded structure depends on position and orientation of the existing sharp weld defect. Different pre-cracked specimens were used in this experimental investigation.

They were cut from the base and weld metals and heat-affected zone. In comparison with the base metal, weld joint region showed higher crack growth rate at operating and room temperatures. Fatigue crack growth rate was higher at operating temperature irrespective of the position. Reliability of structure with initial longitudinal cracks positioned in the heat-affected zone was lower than with initial transversal cracks located in the weld metal.

© 2008 Journal of Mechanical Engineering. All rights reserved.

Keywords: welded structures, fatigue cracks, fracture toughness, proof test

0 INTRODUCTION

Weld defects arise in manufacture of welded structures. During normal operation of such structures, sharp defects in weld joint region act as sites from which fatigue cracks form and then grow. Cracks of critical size jeopardize structural integrity. Due to the complex nature of fusion welding and human factor, the size, location, type, and orientation of defects cannot be predicted. Only a thorough post-manufacture inspection of weld joints provides necessary information about the actual weld defect presence in welded structures.

The most jeopardizing type of sharp weld defects are two-dimensional defects oriented normal to the direction of fluctuating stress. Their direct effects on the strength of weld joints are treated as the effects of cracks (crack-like defects). Fracture mechanics is used to assess the severity of macroscopic two-dimensional defects in relation to design loading. There are some complex features that make the application of fracture mechanics difficult such as residual stresses, interaction of cracks with weld geometry, material properties variations due to

dissimilar weld and base metals and especially microstructural heterogeneities of weld joint region resulting from the welding thermal cycles.

Tensile welding residual stresses appearance and local material embrittlement are fundamental for various cracking phenomena of welds [1]. Interaction of stresses during structure operation and existing cracks often leads to unexpected weld joint fracture. Actually, cracks originating from sharp weld defects grow during service life of welded structures. They have to remain smaller than the critical crack size, otherwise, they will cause weld joint fracture in brittle or quasi-brittle manner. Disintegration of a welded structure is very likely if highly loaded weld joint collapses. A superior resistance of weld joint against the fatigue crack growth is of great importance for longer service lives of welded structures.

The resistance of metallic materials to fatigue crack growth and brittle fracture depends on the microstructure. Properties of the base metal (BM) meet requirements in standards. The weakest links are always weld joints consisting of heat-affected zone (HAZ) and weld metal (WM). Microstructure of both in as-welded condition

*Corr. Author's Address: Institute "GOŠA", Belgrade, Serbia, merib@neobee.net

results from chemical composition and welding thermal cycles.

Microstructure and properties of weld joint region can be analysed in details by using samples of materials cut from actual weld joints [2]. Alternative is an analysis performed with samples of materials with simulated microstructure. In this case, thermal conditions during welding have to be simulated either on samples of BM in order to prepare particular HAZ areas [3] or on samples of single-run WM in order to prepare particular multi-run WM areas [4]. Using combination of both, i.e. samples from weld joint and samples with simulated microstructure is an effective approach, too [5].

The experimental results of fracture toughness measurement and fatigue-crack growth rate measurement are shown and discussed in this paper from the leak-before-break concept point of view. Fracture properties of weld joint region and non-affected base metal were determined using the specimens machined from the samples of material cut from a real welded plate.

1 EXPERIMENTALS

1.1. Materials and Specimens

The steel used in this study is A-387 Gr. 11 Class 1 steel designed for operation at elevated temperatures. Its chemical composition and basic mechanical properties at room temperature are shown in Table 1 [6]. A 96 mm thick double-U

shaped welded test coupon was available for the research. Root passes were deposited by metal manual arc welding (MMA) with coated electrode LINCOLN SI 19G (AWS: E8018-B2), the rest of the weld-groove was filled at both sides by submerged arc welding (SAW) with wire LINCOLN LNS 150 and flux LINCOLN P230. Chemical compositions of both consumables are shown in Table 2. Basic mechanical properties for all-weld metals at room temperature are shown in Table 3 [6]. The WM is stronger than BM (overmatching).

Welding technology specification was prepared according to standard EN 288-3 [7]. Operating temperature is not specified in this standard. It is not required to test the behaviour of the weld joints at the operating temperature.

Weld joint with sharp initial weld defects in the WM and HAZ areas was evaluated in respect of the structure safe operation. The specimens for the fracture toughness assessment and fatigue crack growth rate measurement were machined from the welded test coupon as shown in Figure 1.

Three-point bend specimens (TPB) were used for fracture toughness testing at room temperature. Their shape and dimensions are shown in Figure 2. Due to specific design of the high-temperature chamber, the specimens looked like compact tensile specimens (CT) used for fracture toughness testing at operating temperature. Their shape and dimensions are also shown in Figure 2.

Table 1. *Chemical composition and basic mechanical properties of the steel*

C	Si	Mn	P	S	Cr	Mo	Yield stress	Tensile strength	Elongation	Impact energy
Mass. %							MPa		%	J
0.15	0.29	0.54	0.022	0.011	0.93	0.47	325	495	35	165

Table 2. *Chemical composition of filler metals*

Filler metal	C	Si	Mn	P	S	Cr	Mo
	Mass %						
LINCOLN SI 19G	0.08	0.045	0.35	0.025	0.025	1.10	0.50
LINCOLN LNS 150	0.11	0.18	0.37	0.020	0.020	1.04	0.47

Table 3. *Mechanical properties of all-weld metals*

Filler metal	Yield stress	Tensile strength	Elongation	Impact energy
	MPa		%	J
LINCOLN SI 19G	505	640	23	> 95
LINCOLN LNS 150	490	610	26	> 100

Bending specimens (B) were used for fatigue-crack growth-rate measurement. Their dimensions were 10×10×55 mm. The type of all specimens, their position, and orientation in the test coupon in relation to the weld axis is clearly indicated in Figure 1. The notches and cracks were located in the BM, WM and HAZ.

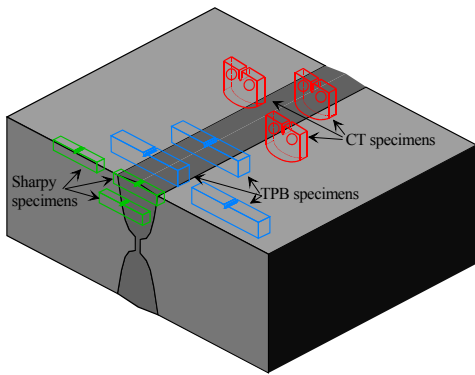


Fig. 1. View of the welded test coupon with specimens sampling

The values of J-integral were calculated from registered dependence of force versus load-point displacement just when unloading sequence started. The diagrams $J - \Delta a$ were plotted using those values and corresponding crack increments. At first, a regression line was drawn in the linear section of each $J - \Delta a$ diagram. J_{Ic} -value, critical J-integral, was obtained with intersecting $J - \Delta a$ diagram and a parallel line to regression line. This line intersects x-axis at $\Delta a = 0.15$ mm. The diagrams $J - \Delta a$ at room and operating temperature valid for the BM are shown in Figs. 3b and 4b, the diagrams valid for the WM in Figs. 5b and 6b, whereas the diagrams valid for the HAZ in Figs. 7b and 8b. Average values of

determined J_{Ic} -values extracted from those diagrams are listed in Table 4 [10].

2 RESULTS

2.1. Fracture toughness

Fracture toughness was experimentally determined according to the standards [8] and [9]. Single-specimen method was used. Three specimens were notched and precracked in the BM, three in the WM and three in the HAZ. The specimens were loaded and successively partly unloaded at room temperature and at 540°C. The registered slope between force, F , and crack mouth opening displacement, δ (CMOD), in the course of specimen unloading enabled determination of the crack size, a , and every crack increment, Δa , respectively. The examples of diagrams $F - \delta$ plotted at room and operating temperature valid for the BM are shown in Figs. 3a and 4a, diagrams valid for the WM in Figs. 5a and 6a, whereas diagrams valid for the HAZ in Figs. 7a and 8a.

The values of J-integral were calculated from registered dependence of force versus load-point displacement just when unloading sequence started. The diagrams $J - \Delta a$ were plotted using those values and corresponding crack increments. At first, a regression line was drawn in the linear section of each $J - \Delta a$ diagram. J_{Ic} -value, critical J-integral, was obtained with intersecting $J - \Delta a$ diagram and a parallel line to regression line. This line intersects x-axis at $\Delta a = 0.15$ mm. The diagrams $J - \Delta a$ at room and operating temperature valid for the BM are shown in Figs. 3b and 4b, the diagrams valid for the WM in Figs. 5b and 6b, whereas the diagrams valid for the HAZ in Figs. 7b and 8b.

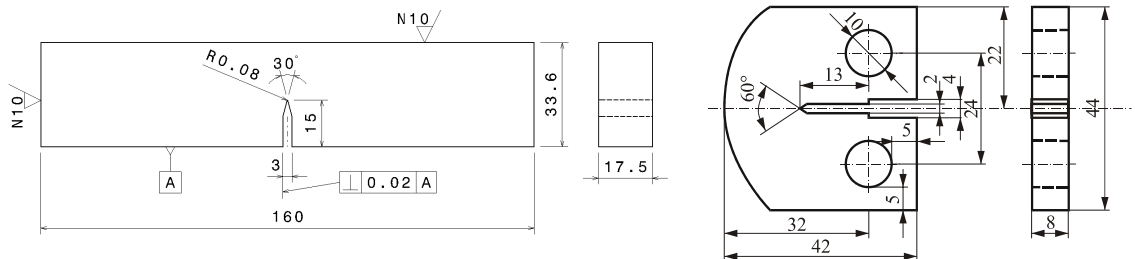


Fig. 2. Fracture toughness specimens (TPB specimens above and “CT” specimens below)

Average values of determined J_{Ic} -values extracted from those diagrams are listed in Table 4 [10].

In respect of fracture toughness the highest

quality area of treated weld joint is WM whereas the lowest HAZ. Testing temperature does not change this fact.

Table 4. Fracture toughness, J_{Ic} , plane-strain fracture toughness, K_{Ic} , threshold stress-intensity range and parameters of fatigue crack growth rate C and m

Area	T, °C	J_{Ic} , kJ/m ²	K_{Ic} , MPa m ^{1/2}	ΔK_{th} , MPa m ^{1/2}	C, nm/cycle	m
BM	20	63.5	120.9	6.8	$4 \cdot 10^{-3}$	2.1
WM		81.3	133.7	6.8	$8 \cdot 10^{-4}$	2.8
HAZ		51.7	106.6	6.7	$2 \cdot 10^{-4}$	3,5
BM	540	43.4	88.4	5.9	$1 \cdot 10^{-3}$	3.0
WM		57.2	101.6	6.2	$5 \cdot 10^{-4}$	3.5
HAZ		38,9	83.7	6.1	$3 \cdot 10^{-4}$	3.9

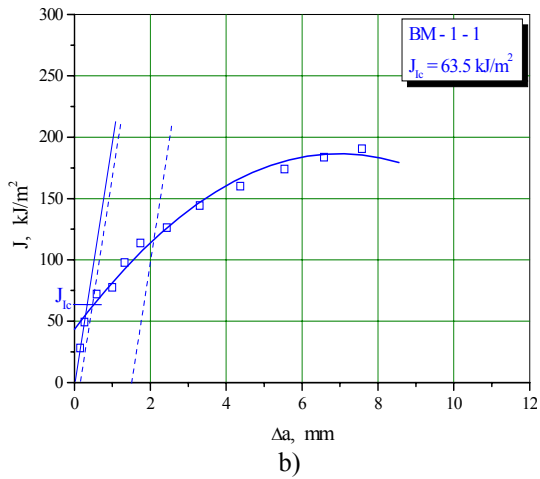
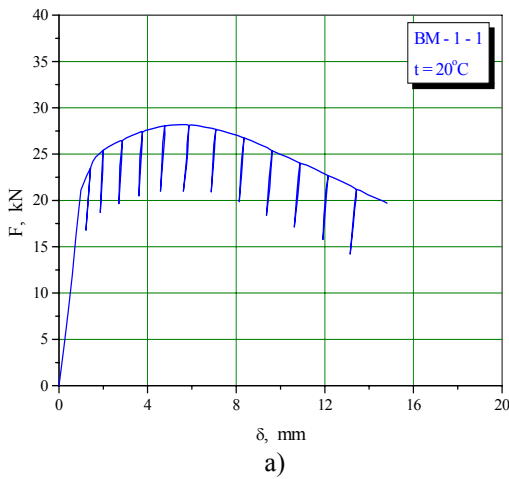


Fig. 3. Diagrams $F - \delta$ and $J - \Delta a$ for the BM at room temperature

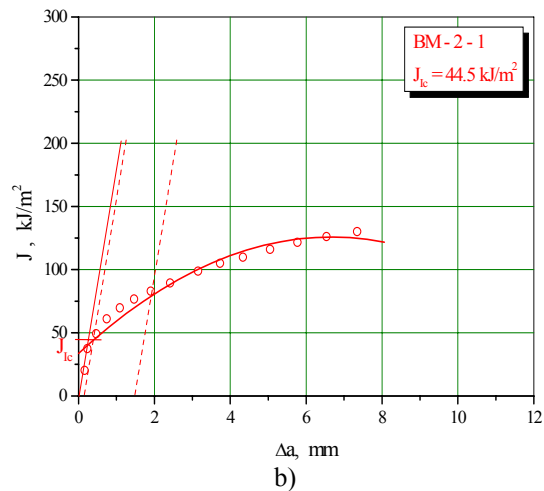
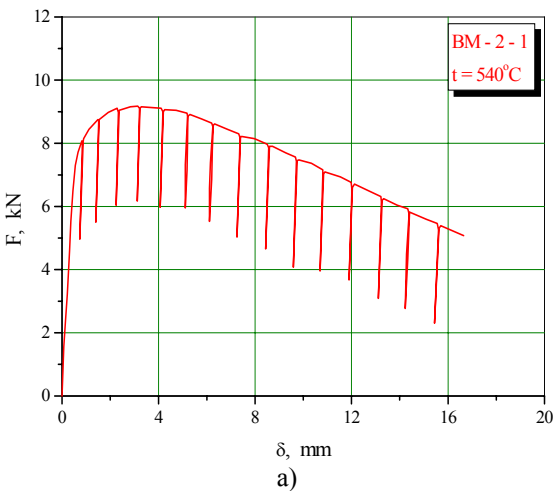


Fig. 4. Diagrams $F - \delta$ and $J - \Delta a$ for the BM at operating temperature

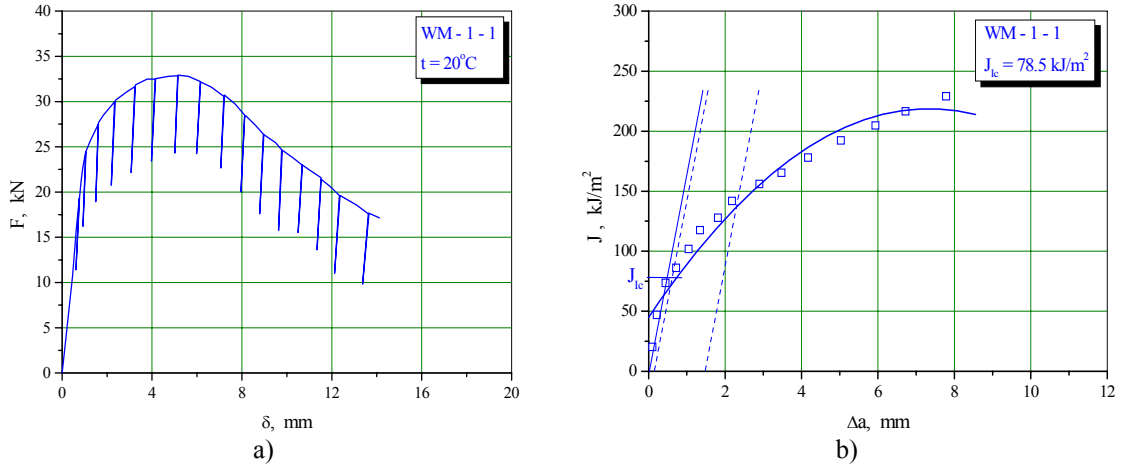


Fig. 5. Diagrams $F - \delta$ and $J - \Delta a$ for the WM at room temperature

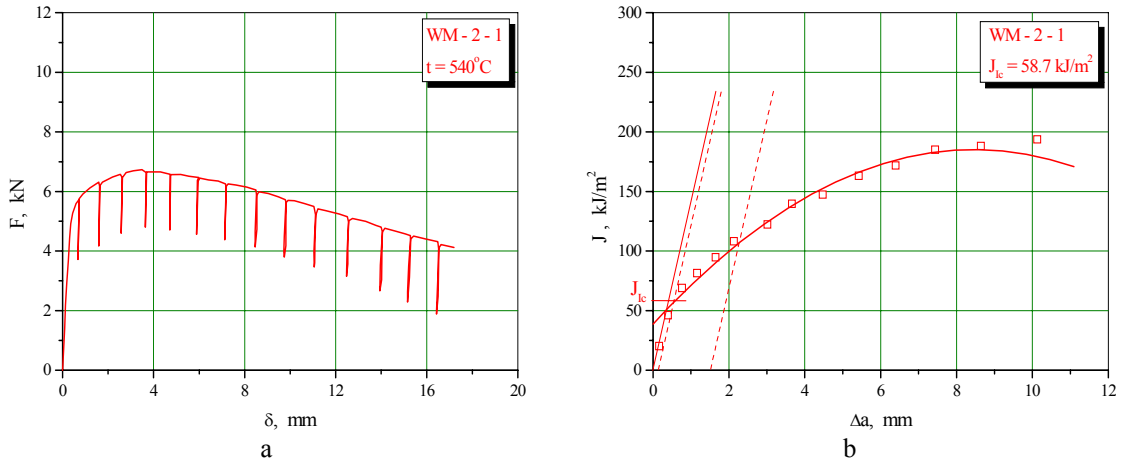


Fig. 6. Diagrams $F - \delta$ (a) and $J - \Delta a$ (b) for the WM at operating temperature

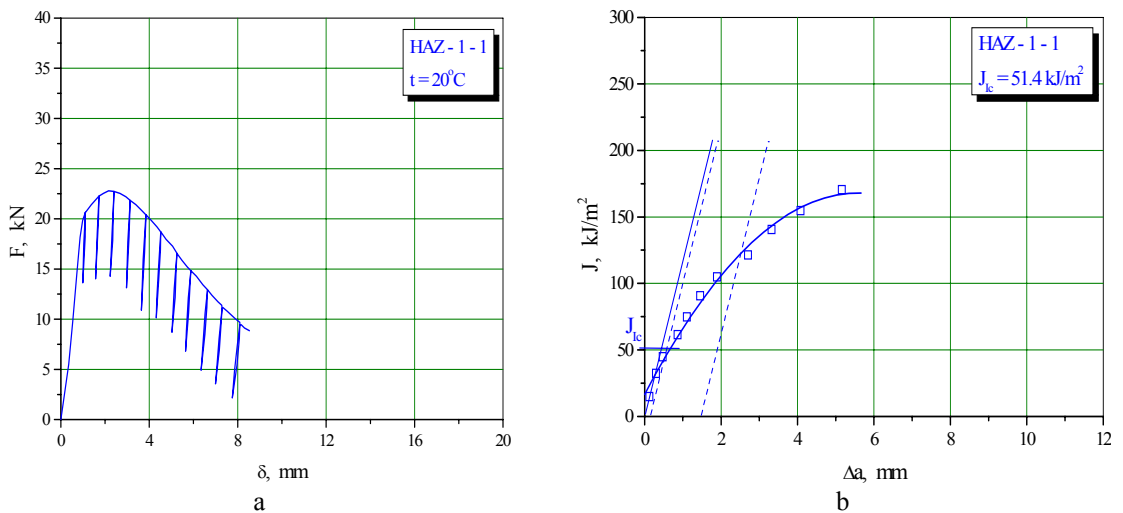


Fig. 7. Diagrams $F - \delta$ (a) and $J - \Delta a$ (b) for the HAZ at room temperature

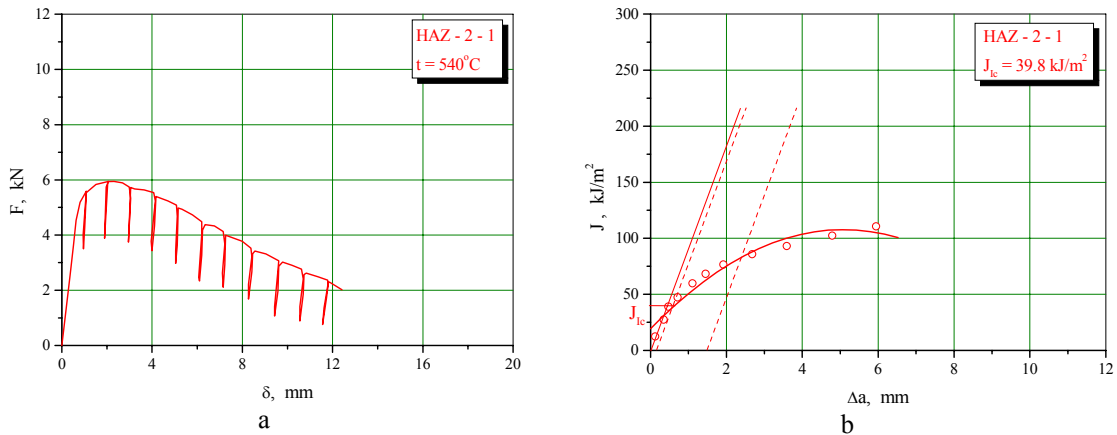


Fig. 8. Diagrams $F - \delta$ (a) and $J - \Delta a$ (b) for the HAZ at operating temperature

2.2. Fatigue-crack growth-rate parameters

Fatigue-crack growth-rate parameters were experimentally determined according to the standard ASTM E 647 [11]. Charpy-size specimens were notched to a depth of 2 mm in the WM and HAZ areas and in the BM. They were bend-loaded in moment control at room temperature and at 540°C on a high-frequency resonant pulsator. Resistant foil-gauges were attached on the specimens in order to register crack size changes during oscillating loading (see Figure 9). In the course of successive small crack increments, the stress-intensity factor range, ΔK , was kept constant. Simultaneous corrections of loading moment were performed during fatigue crack growth. Fatigue crack growth rate, da/dN , was calculated as a quotient of crack increment, Δa , and number of cycles, N .

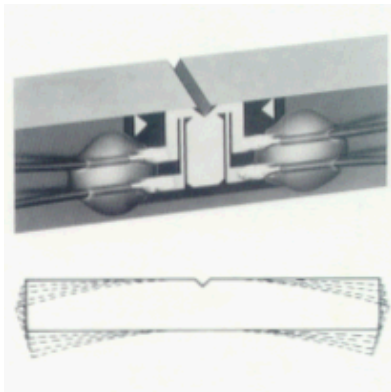


Fig. 9. Specimen with firmly cemented crack size gauge with indicated bend-loading

The fatigue crack growth rate rapidly decreased when ΔK when approaching the threshold stress-intensity factor range, ΔK_{th} . On the other side, when ΔK came up to K_{Ic} -value fatigue crack grew faster.

Experimental diagrams $da/dN - \Delta K$ represented in double-logarithmic scale at room temperature valid for the BM, WM, and HAZ are shown in Figure 10a and those at operating temperature in Figure 10b.

The linear portion of relationship between the fatigue crack growth rate and stress-intensity factor range is known as Paris law [12]:

$$\frac{da}{dN} = C \cdot (\Delta K)^m \quad (1)$$

where constants C and m are material-dependent.

Fatigue-crack growth-rate parameters extracted from diagrams are listed in Table 4 [13].

3 EVALUATION OF TEST RESULTS

If mechanical properties are available, plane-strain fracture toughness, K_{Ic} , is indirectly determined from the J_{Ic} -values. The following expression is used:

$$K_{Ic} = \sqrt{\frac{J_{Ic} \cdot E}{1 - \nu^2}} \quad (2)$$

where E is Young's modulus and ν Poisson's number.

Estimated value of E at temperature of 540°C is 82% of the same value at room temperature [14]. We took the same value of ν at

room temperature and 540°C for the calculation of K_{Ic} -values given in Table 4.

Variations of K_{Ic} in the weld joint region in comparison with BM are extremely significant. Critical crack size, a_c , when weld joint fractures at a fixed stress level is strongly K_{Ic} dependent. By applying formula

$$K_{Ic} = \sigma \cdot Y(a) \sqrt{\pi \cdot a_c} \quad (3)$$

Critical crack size is calculated as

$$a_c = \frac{1}{\pi} \cdot \left(\frac{K_{Ic}}{\sigma \cdot Y(a)} \right)^2 \quad (4)$$

where $Y(a)$ is shape factor and σ stress normal to the crack plane.

When fatigue crack grows in accordance with Paris law, stress-intensity factor range is greater than the threshold stress-intensity factor range, ΔK_{th} .

If the fatigue crack growth rate parameters C and m are available, the number of cycles to fracture, N , will be determined using Equation 1. The following expression has to be solved:

$$\int_{a_i}^{a_f} \frac{da}{Y(a) \cdot a^{\frac{m}{2}}} = C \cdot \pi^{\frac{m}{2}} \cdot (\sigma)^m \cdot \int_0^N dN \quad (5)$$

where a_i and a_f are initial and final crack size, respectively.

Shape factor of an infinite 96-mm thick wall with different types and sizes of cracks are [15]:

- Small half-elliptic surface crack with length-to-depth ratio 2.42 (Figure 11a): $Y = 0.734$
- Half-elliptic surface crack with length-to-depth ratio 2.83 penetrating half of the wall-thickness (Figure 11b): $Y = 0.86$
- Half-elliptic surface crack with length-to-depth ratio 4.2 approaching opposite wall surface (Figure 11c): $Y = 1.234$
- Through-thickness crack (Figure 11d): $Y=1$.

4 DISCUSSION WITH CONCLUSION

If during cyclic loading an existing crack, previously generated from a sharp weld defect, had grown to the size when anywhere along the crack contour stress-intensity factor attains plane strain fracture toughness, K_{Ic} -value, an abrupt fracture of weld joint would occur. This size is defined as the critical crack size. If size of fatigue crack attains the critical crack size, weld joint will fracture. The result can be a catastrophic disintegration of the whole structure.

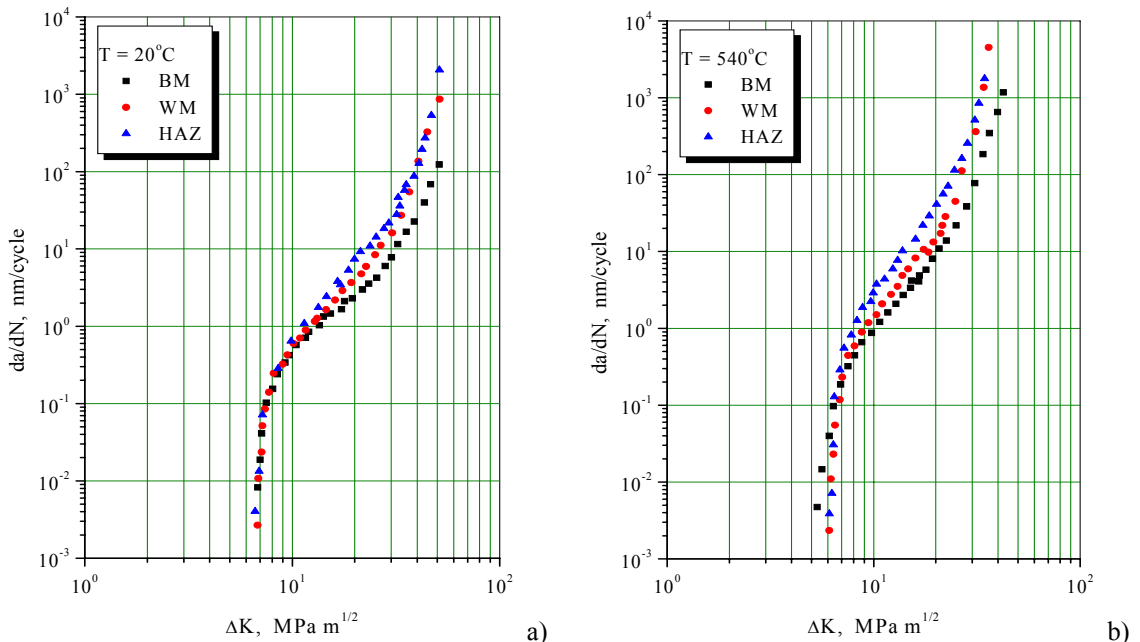


Fig. 10. Diagrams $da/dN - \Delta K$ for the BM, WM, and HAZ at room temperature (a) and at 540 °C (b)

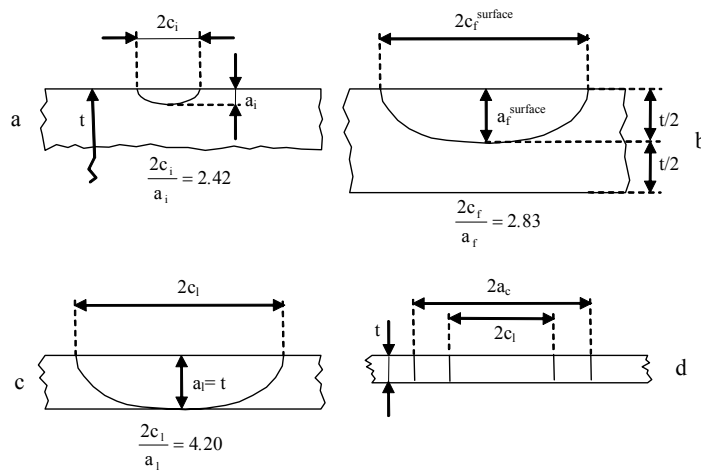


Fig. 11. Four types of fatigue cracks: small initial half-elliptic surface crack a_i (a), final half-elliptic surface crack a_f (b), wall-penetrating crack when leakage starts a_l (c), critical and non-critical through-thickness cracks a_c , c_l (d)

Assume that initial inner surface crack in the weld joint area is already a long crack. For the linear-elastic treatment, the depth of this crack, a_0 , has to be much greater than the plastic zone size, r_y (Figure 11a).

$$a_i \geq 50 \cdot r_y \quad (6)$$

Plastic zone ahead of the crack tip develops as the result of interaction between a crack and stress. Its size depends on the stress-intensity factor, K , material yield stress, R_p , and stress-field configuration.

$$r_y = \left(\frac{K}{R_p} \right)^2 \cdot \begin{cases} \frac{1}{2\pi} & \text{plane stress condition} \\ \frac{1}{6\pi} & \text{plane strain condition} \end{cases} \quad (7)$$

Operating stress of the structure does not exceed 100 MPa. Inner surface crack 5 mm-deep fulfils the condition in Equation 6. Cracks of this size were found in the structure during regular in-service inspections. Therefore, those cracks grow in accordance with Paris law. Proof pressure test performed after in-service inspections led to the stress 100% higher than maximum operating stress.

It is great advantage to operate a pressure-plant designed based on leak-before-break. Fatigue-crack penetration through the wall can be manifested either by loss of pressure or by leakage. Thanks to those obvious indications, an operator is capable to prevent final fracture of the plant by shutting it down. Abrupt fracture of

pressurized component could be jeopardizing for human lives and environment. Besides, a plant designed in accordance with leak-before-break concept allows periodical repairs or replacement of the damaged component.

The procedure is as follows:

- 1) Calculation of the through-thickness crack size which results in fracture, a_c^{through} (subscript c denotes critical size for fracture).
- 2) Calculation of the depth of surface crack in an infinite thick wall which results in fracture, a_c^{surface} infinite 96-mm thick wall
- 3) Comparison of the a_c^{surface} with the wall thickness t . If $a_c^{\text{surface}} < t$, crack will not penetrate the wall in a stable manner before fracture.
- 4) If $a_c^{\text{surface}} > t$, the crack will penetrate the wall. Depth of crack approaching the opposite surface of the wall, a_l , is t , whereas its length $2c_l = 4.2 \times a_l$ (subscript l denotes the size for leakage to start).
- 5) The crack penetrating the wall grows further and becomes a through-thickness crack of length $2a = 2c_l^{\text{surface}}$.
- 6) If the critical crack size $a_c^{\text{through}} \gg a_c^{\text{surface}}$, there is enough time to notice pressure loss or leakage.

Calculated size of part-through and through-thickness critical cracks in BM, WM, and HAZ are listed in Table 5. Sizes a_c^{surface} are greater than wall thickness ($t = 96$ mm). Crack

would certainly penetrate the wall before final fracture.

When crack would approach the opposite wall surface, its half-length on the inner surface would be $c_l = 202$ mm. This is not much less than critical through-thickness crack size under normal operating condition in the BM (249 mm) and especially in the HAZ (223 mm). Without any doubt, weld joint properties of this plant satisfy the leak-before-break concept, but its operating safety factor is a bit questionable.

Calculated critical sizes of the through-thickness crack in proof-test condition are listed in Table 5. They are much smaller than the half-length of the crack penetrating the wall. The possibility that the existing deep crack cannot be detected during in-service inspection after which proof-test should be performed may not be neglected. Crack size $a_c^{through}$ in proof-test condition could be crucial for further safe operation of the plant.

For higher reliability, it is beneficial to limit maximum allowable crack size rigorously, for instance, let the crack size be only one-half of the wall-thickness. Stress-intensity factor which is the result of this crack at proof stress is $K = 67$

MPa. This level of stress-intensity is lower than the plane-strain fracture toughness of BM, WM, and even HAZ. If during in-service inspections a careful effort were made to find all cracks on inner surface, safe operation of plant would be guaranteed.

Which cracks are more dangerous in the weld joint region - longitudinal cracks in the HAZ or transversal cracks in the WM? These cracks are often the result of hydrogen attack on hard areas of weld joints.

In terms of experimental data listed in Table 4, the cracks in the HAZ will grow faster than the cracks in the WM. Initial cracks in the HAZ could grow all the time through the material with the worst properties. Initial cracks in the WM grow at first in the WM, then go across HAZ, and continue outside the weld joint in the BM which properties are superior. Comparison of the number of cycles for an initial 5 mm-deep crack to grow to 50% of the final crack size ($a = 24$ mm) at room and operating temperatures is shown in Table 6. The basis is necessary number of cycles for crack growth in the HAZ at operating temperature.

Table 5. Critical sizes of part-thickness and through-thickness cracks in normal operating and proof test conditions

Area	T, °C	$a_c^{surface}$	c_l	$a_c^{through}$	$a_c^{through}$
		operating condition			proof-test condition
		mm			mm
BM	20	864	202	465	116
WM		1056	202	569	142
HAZ		671	202	362	90
BM	540	462	202	249	62
WM		610	202	329	82
HAZ		414	202	223	56

Table 6. Time needed for the crack growth to half of the final crack size at operating temperature in relation to the time for growth in the weakest area of the weld joint region, i.e. HAZ

Area	T, °C	N/N_0 operating condition
BM	20	51.8
WM		8.8
HAZ		4.5
BM	540	3.8
WM		1.8
HAZ		1

Quotients N/N_0 listed in Table 6 are additional safety factors for the safe structure operation. The most dangerous situation is the presence of longitudinal cracks in the HAZ, which grow through the HAZ under cyclic loading at temperature of 540°C.

5 REFERENCES

- [1] Z. Burzić, S. Sedmak, M. Manjgo (2001) The application of fracture mechanics in welded joint properties assessment, RIM 2001, Bihać, pp. 451-460.
- [2] N. Gubelj (1999) Fracture behavior of specimens with surface notch tip in the heat affected zone (HAZ) of strength mismatched welded joints, International journal of fracture, 100 (2) pp. 155-167
- [3] V. Gliha (2005) The microstructure and properties of materials at the fusion line, Metallurgy, 44 (1), pp. 13-18.
- [4] D. Rojko, V. Gliha (2005) Simulations of transformation kinetics in a multi-pass weld, Materials and manufacturing processes, 20 (5), pp. 833-849.
- [5] I. Rak, V. Gliha, M. Koçak (1997) Weldability and toughness assessment of Ti-microalloyed offshore steel. Metallurgical and materials transactions A, 28, pp. 199-206.
- [6] M. Burzić, Z. Burzić, J. Kurai (2006) The prediction of residual life of reactors in RNP, CertLab Pančevo.
- [7] EN 288-3, (1995) Approval of welding procedures for metallic materials-Part 3: Welding procedure tests for arc welding of steels, Quality assurance in welding, Belgrade.
- [8] ASTM E1152-91 (1995) Standard Test Method for Determining J-R Curve, Annual Book of ASTM Standards, Vol. 04.01. pp. 724.
- [9] BS 7448 (1991) Fracture mechanics toughness tests. Part 1. Method for determination of K_{Ic} critical CTOD and critical J values of metallic materials, BSI.
- [10] M. Burzić (2007) PhD Thesis, University of Novi Sad, Department of Technical Faculty, Serbia.
- [11] ASTM E647 (1995) Standard Test Method for Constant-Load-Amplitude Fatigue Crack Growth Rates Above 10^{-8} m/cycle, Annual Book of ASTM Standards Vol. 03. 01, pp. 714.
- [12] P.C. Paris, and F. Erdogan (1982) A Critical Analysis of Crack Propagation Laws, Trans. ASME, Journal Basic Eng., Vol. 85, No. 4, pp. 528.
- [13] M. Burzić, Z. Burzić, J. Kurai, Dž. Gačo (2007) Fatigue Behaviour of Alloyed Steel for High Temperature, First Serbian (26th YU) Congress on Theoretical and Applied Mechanics, Kopaonik, Serbia, pp. 1085-1090.
- [14] DIN 4133 (1991) Schornsteine aus Stahl, Berlin.
- [15] Y. Murakami, (1986), Stress Intensity factors Handbook, Pergamon Press.